Increasing the density of nanomedicines improves their ultrasound-mediated delivery to tumours

CrossMark

Steven Mo [a], Robert Carlisle [a,*], Richard Laga [b,c], Rachel Myers [a], Susan Graham [a], Ryan Cawood [b], Karel Ulbrich [c], Leonard Seymour [b], Constantin-C. Coussios [a]

[a] Institute of Biomedical Engineering, Department of Engineering Science, University of Oxford, Old Road Campus Research Building, Oxford OX3 7DQ, UK
[b] Clinical Pharmacology, Department of Oncology, University of Oxford, Old Road Campus Research Building, Oxford OX3 7DQ, UK
[c] Institute of Macromolecular Chemistry, Czech Academy of Sciences, Prague, Czech Republic

ARTICLE INFO

ABSTRACT

Nanomedicines have provided fresh impetus in the fight against cancer due to their selectivity and power. However, these agents are limited when delivered intravenously due to their rapid clearance from the bloodstream and poor passage from the bloodstream into target tumours. Here we describe a novel stealthing strategy which addresses both these limitations and thereby demonstrate that both the passive and mechanically-mediated tumour accumulation of the model nanomedicine adenovirus (Ad) can be substantially enhanced. In our strategy gold nanoparticles were thoroughly modified with 2 kDa polyethyleneglycol (PEG) and then linked to Ad via a single reduction-cleavable 5 kDa PEG. The resulting Ad–gold–PEG construct was compared to non-modified Ad or conventionally stealthed Ad–poly[N-(2-hydroxypropyl)methacrylamide] (Ad–PHPMA). Notably, although Ad–gold–PEG was of similar size and surface charge to Ad–PHPMA the increase in density, resulting from the inclusion of the gold nanoparticles, provided a substantial enhancement of ultrasound-mediated transport. In an in vitro tumour mimicking phantom, the level and distance of Ad–gold–PEG transport was shown to be substantially greater than achieved with Ad–PHPMA. In in vivo studies 0.1% of an unmodified Ad dose was shown to accumulate in tumours, whereas over 12% of the injected dose was recovered from the tumours of mice treated with Ad–gold–PEG and ultrasound. Ultimately, a significant increase in anti-tumour efficacy resulted from this strategy. This stealthing and density-increasing technology could ultimately enhance clinical utility of intravenously delivered nanoscale medicines including viruses, liposomes and antibodies.

1. Introduction

Intravenous (IV) delivery of nanomedicines to tumours is sub-optimal due to instability in the bloodstream and poor penetration from the bloodstream and deep into tumours [1–3]. Interactions with bloodstream components have recently been more clearly defined for a range of nano-agents such as liposomes, nanoparticles and adenoviruses (Ad) [4–6]. Such studies have helped the development of chemical modification strategies which utilises polyethyleneglycol (PEG) or poly[N-(2-hydroxypropyl)methacrylamide] (PHPMA) polymers to reduce blood component binding and thereby improve circulation kinetics [7–11]. However, such chemical 'stealthing' often provides insufficient protection to allow optimal activity of these nanomedicines, or modifies them to such an extent that their activity at the target site is compromised [7,12]. Furthermore, although uptake of nano-sized agents into target

tumours benefits from the enhanced permeability retention effect (EPR) [13,14], such passive accumulation still only permits 1–2% of the injected dose to accumulate. In response, device based approaches providing physical/mechanical stimuli to actively drive nanomedicines from the circulation deep into tumours have gained prominence, with application of focussed ultrasound being recognised as a particularly attractive option [15–17].

Here we describe an approach which provides enhancement of both EPR assisted passive accumulation as well as device based mechanical transport to tumours. Specifically, gold nanoparticles were sparsely modified with 5 kDa PEG and then heavily modified with 2 kDa PEG. The resulting novel 'dandelion' construct was linked via a reduction labile disulphide bond to the nanomedicine adenovirus, to give Ad–gold–PEG (see Graphical abstract). Gold nanoparticles are an ideal nanomedicine component due to their biocompatibility, low toxicity and amenability to surface modification.

Our dandelion-like structure provided a thick protective steric shield of 2 kDa PEG similar to that achieved with multivalent PHPMA-based polymers whilst still relying on one-point attachment of the

* Corresponding author.
E-mail address: robert.carlisle@eng.ox.ac.uk (R. Carlisle).
URL: http://www.ibme.ox.ac.uk/bubbl (R. Carlisle).

shield to the adenovirus (via the 5 kDa PEG), as with conventional PEG coating. The disulphide bond between the adenovirus and the gold-PEG provided a mechanism for triggered de-stealthing and infection reactivation within reducing environments found within tumours [18,19]. Attachment of the dense steric shield via a minimal number of reducible 5 kDa PEG links was designed to allow effective de-shielding. Crucially, the addition of gold nanoparticles also substantially increased the density of the Ad construct, thereby enhancing its response to focussed ultrasound induced cavitation events. This strategy has the potential to broaden the clinical utility of powerful therapeutic agents by enabling their successful delivery following IV injection for cancer treatment.

2. Materials and methods

2.1. TNBS assay

A TNBS (2,4,6-Trinitrobenzenesulfonic acid) assay was used to determine depletion of amine groups on gold and Ad particles in response to addition of amine reactive PEG, PHPMA or gold–PEG [20]. In brief, standard curves of unmodified gold or Ad were treated identically to samples and TNBS added before absorbance at 335 nm was measured.

2.2. Synthesis of Ad–gold–PEG

A sample of 1×10^{14} spherical amine-presenting 5 nm gold (~300 amine groups per gold particle; Nanopartz, USA) was first conjugated to 5 kDa carboxyl-PEG-thiol (Rapp Polymere, Germany) via EDC crosslinker chemistry in 1 mL PBS (pH 4.5) at a molar ratio of 1 gold:10 5 kDa-PEG:50 EDC for 1 h at 25 °C. Amicon ultra-4 centrifugal filter (GOLD-CF; Millipore, UK) with molecular weight cut-off of 100 kDa was used to filter out excess 5 kDa-PEG. A TNBS assay was used to determine loss of amine groups from the gold surface and thereby demonstrate that on average 5 molecules of 5 kDa were attached per gold. 5 kDa-thiol-PEG–gold was later conjugated to 2 kDa methyl ether-PEG-N-hydroxysuccinimide (Rapp Polymere, Germany) in 1 mL PBS (pH 7.4) at a molar ratio of 1×5 kDa-PEG–gold:2000 2 kDa-PEG for 2 h at 25 °C. GOLD-CF was again used to filter out excess 2 k-PEG. TNBS confirmed the presence of an average of 257 molecules of 2 kDa PEG per gold nanoparticle. Gold nanoparticles fully saturated with the 2 kDa-PEG-methyl ether and 5 kDa-PEG-thiol (gold–PEG) were reduced in 1 M DTT buffer (pH 8) for 30 min to break any possible disulphide bonds formed, and purification was performed by GOLD-CF. Gold–PEG was reacted with heterobifunctional reagent SPDP in 1 mL PBS (pH 7.4) at a molar ratio of 1 gold–PEG:5000 SPDP for 1 h at 25 °C and purified by GOLD-CF. The final conjugation step was to react gold–PEG–SPDP with adenovirus-type 5 ΔE1/E3 CMV-GFP (Ad; the Native Antigen Company, UK) or Oncolytic Ad [21] in PBS (pH 7.4) at molar ratio of 1 Ad:2000 gold–PEG–SPDP for 1 h at 25 °C. Final Ad–gold–PEG particles were further purified by gel filtration on a Sepharose CL-4B column equilibrated with PBS (pH 7.4) and concentrated to 1×10^{8} viral particles/μL in PBS with 10% glycerol for storage at 4 °C. The % yield for Ad was 30% to 50%.

2.3. Characterization of Ad–gold–PEG

Dynamic light scattering and zeta potential data were obtained at room temperature (RT) in PBS using Zetasizer Nano ZS instrument (Malvern, UK). For TEM analysis, Ad samples were put on formvar-coated 400 mesh copper grids (3.05 mm diameter; TAAB Laboratories Equipment Ltd, UK) for 10 min; the grids were then stained with 2% glutaraldehyde for 5 min, washed with 5 μL of ddH$_2$O twice, stained with 0.5% uranyl acetate for 1 min, and irradiated under the UV light (254 nm) for 10 min before being imaged under tomographic transmission electron microscope (model A-7650; Hitachi, Japan). The TEM magnification was 70,000× at the accelerating voltage of 100 kV. The processing of Ad for TEM leads to the loss of fibre protein from the capsid and so TEM gives a smaller capsid diameter compared to the hydrodynamic diameter measured by DLS. ELISA experiments were carried out as previously described [22]. In vitro experiments in which IGROV-1 and SKOV-3 were infected with Ad or Ad–gold–PEG were carried out in 96-well cell culture plates as previously described [4]. Some slight modifications included: for the IGROV-1 infection experiment, Ad and Ad–gold–PEG were exposed to reducing buffer ranging from 0 mM to 10 mM β-mercaptoethanol (BME) for 20 min; 10 mM BME was chosen as the highest level of reducing buffer because it has a reduction potential of −260 mV (pH 7) [23] which matches the reduction potentials of many reported tumour micro-environments [19,24]. GFP encoded by the Ad, and expressed in IGROV-1 or SKOV-3 cells upon successful infection, was used to measure the efficacy of infection for each sample using a FACSCalibur flow cytometer (Becton Dickinson, UK). SDS-PAGE silver staining was performed as in [7]. In vitro ultrasound experiments were performed using IGROV cells grown in 1% agar within and OptiCell pre-drilled to allow the formation of a flow channel, Ad sample and SonoVue were administered as a continuous infusion through the channel during the ultrasound exposure conditions described in Supplementary Information Fig. S4.

2.4. Synthesis of Ad–PEG and Ad–PHPMA

The synthesis of Ad–PEG [25], PHPMA, and Ad–PHPMA [26] was carried out as previously described. The characterization of PHPMA showed that it contained 6.2 M% of thiazolidine-2-thione reactive groups in side chains and had a molecular weight of 37,000 g/mol. In brief for PEGylation; 25 μL of 40 mg/mL of 20 kDa NHS-PEG in DMSO was added to 1 mL of HEPES (pH 7.4, 50 mM) with 1×10^{11} copies of Adenovirus (= 1 Ad per 300,000 PEG) for 2 h at RT. PEG of 20 kDa was used to provide a mean size similar to that of Ad–gold–PEG and Ad–PHPMA and for extended circulation in accordance with the findings of Doronin et al. [8]. For PHPMA, 20 mg/mL in HEPES (pH7.4, 50 mM) was added to 1×10^{11} copies of Ad for 2 h at RT.

2.5. In vivo bio-distribution and circulation tests of modified Ad on mouse models

CT26 or HepG2 cells were maintained with DMEM cell culture media (10% FBS). Five-week-old BALB/c female mice were obtained from the BMSU of the John Radcliffe Hospital (Oxford, UK). Each mouse was subcutaneously implanted with 5×10^5 CT26 or 5×10^6 HepG2 cancer cells into the flank. Once the tumours reached 100 to 150 mm^3, mice were dosed with 150 μL clodronate liposomes (ClodronateLiposomes.com, Netherlands). 24 h later, mice were randomly divided into eight groups of four mice, and each group was IV dosed with 1×10^{10} Ad, Ad–PEG, Ad–PHPMA, or Ad–gold–PEG. 20 μL blood samples were taken 5, 15, and 30 min after Ad injection and diluted to 200 μL in PBS. Quantitative PCR (Q-PCR) was used to detect the presence of Ad DNA in extracted DNA samples. tumour and liver samples were extracted following cull at 35 min and DNA isolated and quantified as in [4]. In all cases the quantity of adenovirus genomes in the blood, liver and tumour accounted for 95–100% of the total injected dose. In ultrasound experiments parameters and regimes were as in [17]. The ultrasound frequency and range of pressures used in the present study are comparable to those used in a number of recent studies seeking to enhance drug delivery to solid tumours other than in the brain [27]. Animal experimentation was performed according to UK Home Office guidelines and the UKCCCR Guidelines for Welfare of Animals in Experimental Neoplasia.

2.6. Statistical tests

Analyses used ANOVA followed by Newman–Keuls test for pairwise comparison of sub-groups, *, **, and *** represent p-value < 0.05, 0.01, and 0.001, respectively. Data is representative of at least two experiments.

3. Results

3.1. Formulation of gold–PEG and Ad–gold–PEG

Successful coating of Ad with reduction-cleavable gold–PEG was demonstrated using dynamic light scattering (DLS), zeta (ζ) potential, transmission electron microscopy (TEM), and SDS-PAGE silver staining, (Fig. 1). Initial DLS analysis (Supplementary Fig. S1) showed gold–PEG had a greater hydrodynamic diameter (15 nm) than gold (6.3 nm). Unmodified Ad measured 117 nm, Ad–gold–PEG also comprised a single mono-disperse population but measured 149 nm on average, a 32-nm increase which corresponds to the combined size of addition of two gold–PEG, demonstrating a good gold–PEG coating geometry. DLS analysis of identically processed but non-linked Ad and gold–PEG ("Ad + gold–PEG") distinguished two peaks with means of 18 nm for gold–PEG and 114 nm for Ad (Fig. 1A). Treatment of Ad–gold–PEG with reducing agent beta-mercaptoethanol (BME) cleaved the 5 kDa PEG which could then be removed by filtration to return the Ad to its original size. The ζ-potential of gold became less positive (2.6 vs 0.2 Mv) after modification, as amine groups on the gold were removed by reaction with PEG. The ζ-potential of Ad changed from − 16.9 to − 10.8 mV upon reaction with gold–PEG (Supplementary Fig. S1).

Alteration to adenovirus capsid protein size after stealthing with gold–PEG was characterized by separating the proteins by SDS-PAGE. The resulting silver stain (Fig. 1B) indicated that neither Ad (lanes 1 and 2) nor Ad + gold–PEG (lanes 5 and 6) showed a marked difference in Ad protein band intensity in the presence or absence of reducing buffer. In contrast, analysis of Ad–gold–PEG (lanes 3 and 4) showed a substantially different band migration pattern depending on the presence or absence of reducing buffer. Notably, in the absence of reducing agent (lane 4) there was relatively little migration of any Ad protein into the gel, indicating that Ad protein was bound to gold–PEG and unable to properly penetrate the polyacrylamide. However, upon

exposure to reducing buffer (lane 3), Ad–gold–PEG showed equivalent protein migration and intensity to that of Ad and non-linked Ad + gold–PEG, signifying the reduction-induced breakage of disulphide bonds between Ad and gold–PEG to un-stealth Ad to its original form. Analysis of TEM images, as represented in Fig. 1C, showed an average of 60 gold–PEG constructs per Ad capsid. Notably, because the 36 fibre monomers are lost from Ad during TEM processing any gold–PEG attached to these regions cannot be visualised by this method. However, as SDS-PAGE demonstrated that sufficient gold–PEG was attached to each of the 36 fibre monomer proteins to prevent their migration it is reasonable to calculate that at least 36 gold–PEG were attached to fibre proteins (but not detected by TEM). Adding the capsid (60) and fibre values (36) gives a total of approximately 96 gold–PEG per Ad. Notably, TNBS analysis (Supplementary Fig. 2) showed the loss of 111 amine groups from Ad upon reaction with gold–PEG. These analyses therefore indicate that this dandelion stealthing procedure enables the overwhelming majority of each of at least 96 gold–PEG to be linked to Ad by just one 5 kDa PEG molecule.

3.2. Level of protection provided by Ad–gold–PEG stealthing

The biological consequences of the physicochemical changes which were analysed in Fig. 1, were assayed using ELISA and infection of cancer cell lines. ELISA using an anti-Ad antibody demonstrated a significant (p < 0.001) decrease in antibody binding to Ad–gold–PEG compared to Ad and Ad + gold–PEG samples (Fig. 2A). Ad–gold–PEG showed >10-fold lower (p < 0.001) binding to human blood cells after mixing with whole human blood for 30 min at 37 °C, confirming efficient stealthing was achieved (Supplementary Fig. S2B). This indicates good protection of Ad from antibody and classical complement pathway mediated sequestration by erythrocytes and leukocytes when gold–PEG is used [4,29]. Studies in human ovarian carcinoma IGROV-1 cells (which expresses high levels of the Coxsackievirus and Adenovirus
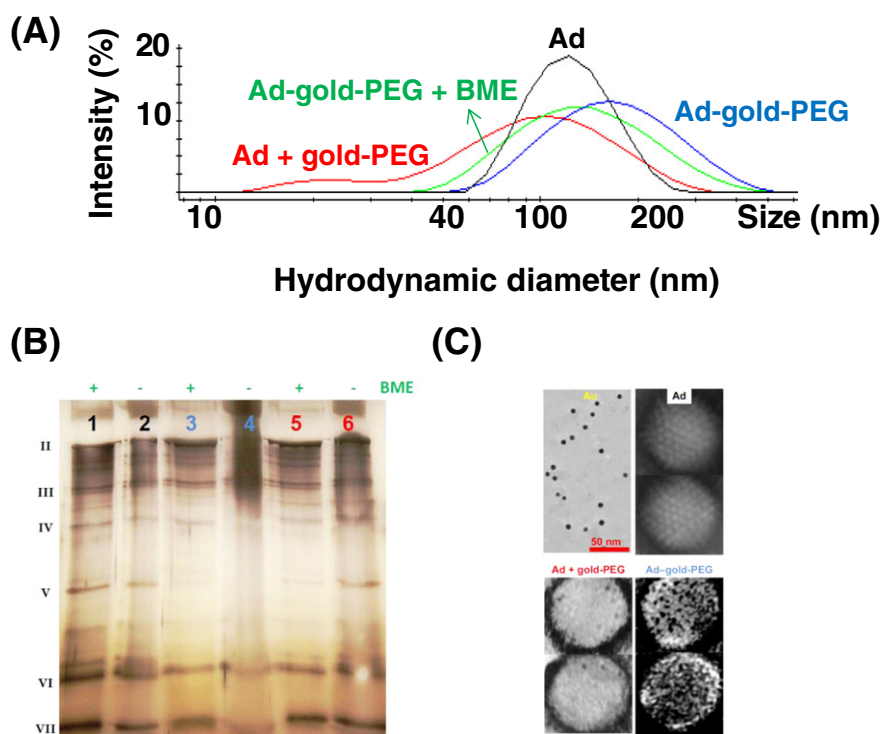

Fig. 1. Modification of gold with PEG and Ad with gold–PEG. (A) Dynamic light scattering showing the mean diameter of gold, gold–PEG, Ad, Ad mixed with gold–PEG (Ad + gold–PEG), and Ad conjugated to gold–PEG (Ad–gold–PEG), or conjugated Ad–gold–PEG treated with betamercaptoethanol (BME) and purified to remove cleaved gold–PEG. (B) Gel electrophoresis showing reduction-reversible retarded migration of Ad proteins following conjugation to gold–PEG. SDS-PAGE silver staining was performed + or − 'BME' reducing buffer (50 mM), lanes 1 and 2 = Ad, 3 and 4 = Ad–gold–PEG, 5 and 6 = Ad + gold–PEG. Roman numerals denote positions of Ad proteins according to MWt [28]. (C) Representative TEM images of gold–PEG ('Au'), Ad, mixed Ad + gold–PEG or conjugated Ad–gold–PEG, images taken at the same magnification, scale bar = 50 nm.
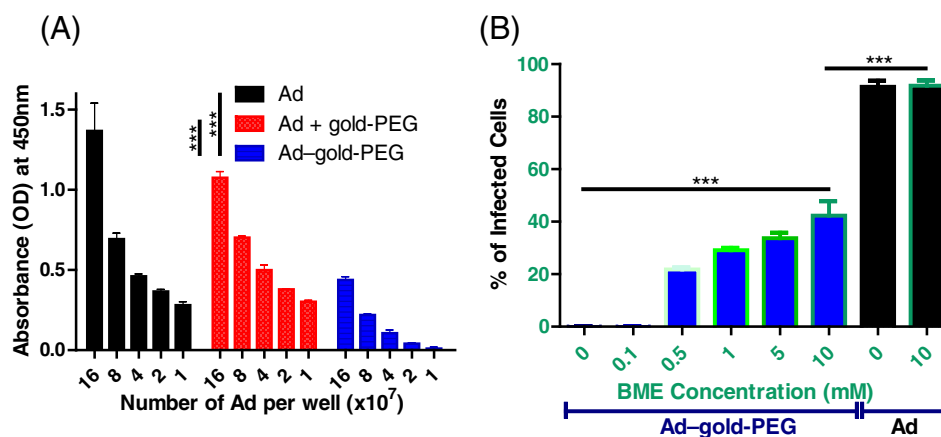
Fig. 2. Gold–PEG for protection against anti-Ad antibody binding and cell infection. (A) Serial dilutions of sample were made and an ELISA using anti-Ad antibodies performed. Ad = non-modified Ad, Ad + gold–PEG = control non-linked Ad and gold–PEG, Ad–gold–PEG = chemically conjugated Ad and gold–PEG. N = 5, SD shown. Analysis by one way ANOVA, *** = at equivalent dilutions for all samples p < 0.001. (B) The utility of the reduction sensitive cleavage and un-stealthing mechanism was demonstrated by infecting with Ad or Ad–gold–PEG which had been pre-incubated with a range of concentrations of the reducing agent BME and assaying expression of the GFP transgene encoded by the Ad, in terms of % of cells positive for GFP. N = 4, SD shown.

Receptors − CAR) showed substantially reduced infection activity for Ad–gold–PEG, indicating that good stealthing of the Ad fibre domain which binds to CAR had been achieved (Fig. 2B). Furthermore, the utility of the disulphide bond as a de-stealthing mechanism was confirmed as 42% of the infectivity of Ad–gold–PEG could be reactivated upon 20 min exposure to a reducing potential matching that of the extracellular tumour milieu [19,23,24]. However, despite BME providing complete removal of gold–PEG and thereby returning the Ad–gold–PEG to the size and charge of non-modified Ad (DLS and zeta potential, Fig. 1) full recovery of infection activity was not possible. This may be due to the presence of thiol adducts which remain on the Ad surface post-cleavage of the gold–PEG.

3.3. Passive accumulation of Ad–gold–PEG to tumours

Over a decade of research has produced two current, but never directly compared, benchmark technologies for Ad stealthing; the use of PEG [30] and the use of PHPMA [26]. Before testing the passive tumour accumulation of novel Ad–gold–PEG constructs, conventionally stealthed Ad–PEG and Ad–PHPMA were prepared [25,31] to allow comparison to these accepted alternative strategies. Sizes and zeta potentials were measured to ensure polymer coating was achieved. Notably, as Ad–PEG, Ad–PHPMA and Ad–gold–PEG have very similar mean diameters which measure in excess of the gaps in the sinusoidal endothelium of both human and mouse liver [32], it may be expected that they would experience the same level of passive removal on passage through the liver. However, when compared by ELISA, Ad–gold–PEG showed much more effective stealthing against the binding of anti-Ad antibodies (Supplementary Fig. S3). In vivo studies were performed in tumour-bearing murine models. After IV dosing of Ad, Ad–PEG, Ad–PHPMA or Ad–gold–PEG, blood samples were taken and tumour and liver samples extracted. Blood circulation profiles of Ad, Ad–PEG, Ad–PHPMA and Ad–gold–PEG are shown in Fig. 3.

Ad, Ad–PEG and Ad–PHPMA circulation data was comparable to previous published results [26,33]. The half-life of Ad–gold–PEG was >30 min, meaning it outperformed all other groups, including Ad–PHPMA. By 6 h post-injection negligible Ad and Ad–PEG, and approximately 10% of Ad–gold–PEG and Ad–PHPMA remained in the circulation and by 24 h less than 1% remained. Ad clearance in mice has been shown to result from extravasation through hepatic sinusoidal endothelia, leading to infection of hepatocytes, and via capture by Kupffer cells [34]. These PK data indicate that the superior stealthing achieved with Ad–gold–PEG, as demonstrated in vitro by ELISA, impacted directly on circulation and hepatic capture in vivo. Crucially, TNBS analysis shows

that this improved stealthing with Ad–gold–PEG was achieved with modification of just 111 capsid amine groups compared to 1332 with Ad–PHPMA or 1007 with Ad–PEG (Supplementary Fig S2). In addition, for the first time in over a decade of development, we are able to show a direct comparison of the blood circulation of Ad–PEG and Ad–PHPMA and confirm the relationship between the improved stealthing with PHPMA (Supplementary Fig. S3) and the improved circulation kinetics (Fig. 3A) compared to conventional PEGylation. Bio-distribution of Ad, Ad–PEG, Ad–PHPMA, and Ad–gold–PEG is represented in Fig. 3B (liver) and Fig. 3C (tumour). More than 90% of Ad and Ad–PEG was captured by the liver. In contrast, liver capture of Ad–PHPMA and Ad–gold–PEG decreased to 48% and 21%, respectively. Furthermore, 9-fold more Ad–gold–PEG than Ad was recovered from the tumour. This is the highest level of passive tumour accumulation that we have ever achieved using this murine model. Integration of the areas under the curve (AUC) for each sample in Fig. 3C and plotting of these data with their respective total Ad accumulated per gramme of tumour, produced a strong correlation (Fig. 3D, R^2 = 0.6968), indicating that passive tumour accumulation of adenovirus is dependent on its plasma AUC. This shows that the enhanced chemical coating and protection of Ad–gold–PEG leads to lower liver capture and extended circulation and ultimately EPR-mediated accumulation. It is notable that these in vivo experiments were performed in mice that had been pre-dosed with clodronate liposomes. Such treatment is a clinically approved means of depleting macrophages and has long been recognised as an effective way of enhancing the circulation kinetics of unmodified Ad and polymer coated Ad in mice [26]. This also mimics current clinical practice whereby 'pre-dosing' with a vector has been used to deplete macrophages and improve the pharmacokinetics of a subsequent 'therapy dose' of the same vector [35]. The advantage of using clodronate to achieve the same macrophage depletion in preclinical tests is that QPCR measurement of the pharmacokinetics of the therapy dose is not compromised by residual pre-dose.

3.4. Increased density of Ad–gold–PEG increases response to focussed ultrasound in vitro

Experiments were performed to test if the presence of gold–PEG could increase adenovirus response to focussed ultrasound and consequently provide improved mechanically-mediated transport into tumours. We and others have demonstrated that exposing tumours to ultrasound provides a powerful stimulus for the movement of nanomedicines from the bloodstream deep into tumours [16,17,36,37]. Here we demonstrate that increasing the density of a nanomedicine such as adenovirus by its attachment to gold–PEG increases its response
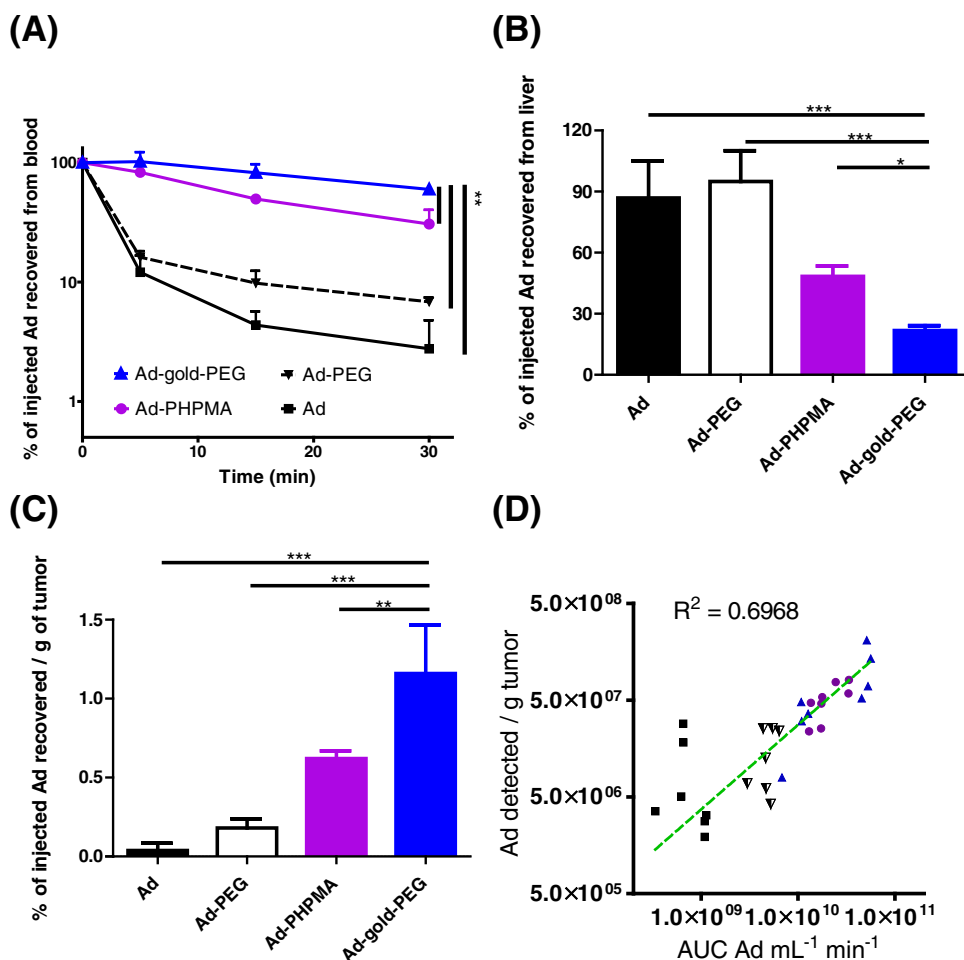
Fig. 3. In vivo circulation assessment of injected Ad, Ad–PEG, Ad–PHPMA, and Ad–gold–PEG. 1×10^{10} copies of sample were injected IV into BALB/c mice bearing CT26 tumours. (A) blood sampling and quantification by QPCR. n = 4, SD shown. Ad–gold–PEG, statistically different from all other groups $p < 0.005$. (B) Total % of the injected dose accumulated in livers. (C) Total % of dose accumulated per gramme of tumour mass; (n = 4), SD shown. Groups compared using ANOVA followed by Newman–Keuls test for pairwise comparison of sub-groups; * and *** represents p-value < 0.05 and 0.001, respectively. (D) Relationship between Ad plasma circulation profile and tumour accumulation. Each point represents one mouse treated with Ad (black square), Ad–PEG (white/black triangle), Ad–PHPMA (purple circle), and Ad–gold–PEG (blue triangle). Area under curve calculated from circulation data at 30 min time point for all mice, N = 8.

to ultrasound induced acoustic cavitation events (Fig. 4). There are no previous reports where nanoparticle density has been modified to enhance response to focused ultrasound, although theory and work using ballistics to deliver micro-particles transdermally [38] is in accordance with our data.

Despite measuring similar diameters Ad, Ad–PHPMA and Ad–gold–PEG showed dramatically different ultra-centrifugation separations, with 99% of Ad–gold–PEG being recovered from the bottom of the tube (Fig. 4A). This is in accordance with the theoretical increase in density from Ad (1.37 g/mL) to Ad–gold–PEG (3.35 g/mL). When applied through a flow channel in a tissue mimicking material (TMM) and exposed to ultrasound in the presence of ultrasound contrast agent SonoVue (set-up in Supplementary Fig. S4) the amount of movement into the TMM scaled with the amount of ultrasound induced inertial cavitation events (as measured by passive cavitation detection [39]) (Fig. 4C–D). Substantially more Ad–gold–PEG, than Ad or Ad–PHPMA moved into the TMM at all penetration depths tested. At a pressure of 1250 kPa 50 to 100-fold more Ad–gold–PEG was recovered at distances of 4 and 6 mm from the flow channel. These data demonstrate that modulating nanomedicine density can alter response to ultrasound and provide precise control over the depth of penetration, which has important implications for the delivery of nanomedicines to tumours as well as transdermally for vaccination. Exposure to BME and analysis of the cells within the TMM for Ad encoded GFP gene expression confirmed

that Ad–gold–PEG maintained infection capacity and had journeyed further than the Ad, whilst also demonstrating that the ultrasound parameters caused no cell damage (Supplementary Fig. S5). A significant increase ($p < 0.001$) in the depth of infection was observed (Supplementary Fig. S6). Notably, in contrast to Ad, infection was only evident with Ad–gold–PEG when reducing agent BME was used, suggesting enhanced selectivity for the tumour environment and therefore safety.

3.5. Passive accumulation and mechanical transport of Ad–gold–PEG in vivo

Experiments were performed to test whether the enhanced passive accumulation of Ad, achieved as a result of improved stealthing with gold–PEG, could be combined with the increased ultrasound-mediated mechanical transport, achieved as a result of the increased density provided by stealthing with gold–PEG. As studies in Figs. 2 and 3 had proven the superiority of Ad–gold–PEG vs Ad–PEG and Ad–PHPMA these groups were no longer included.

Cancer cell killing oncolytic Ad was mixed with luciferase reporter Ad as in [21] and then modified with gold–PEG or not and delivered IV with the cavitation nuclei SonoVue to pre-clinical models (Fig. 5). tumours were exposed to ultrasound regimes as in [17] to create inertial cavitation (see detection in Supplementary Fig. S7), or not, and biodistribution then assayed. This previous study had demonstrated these
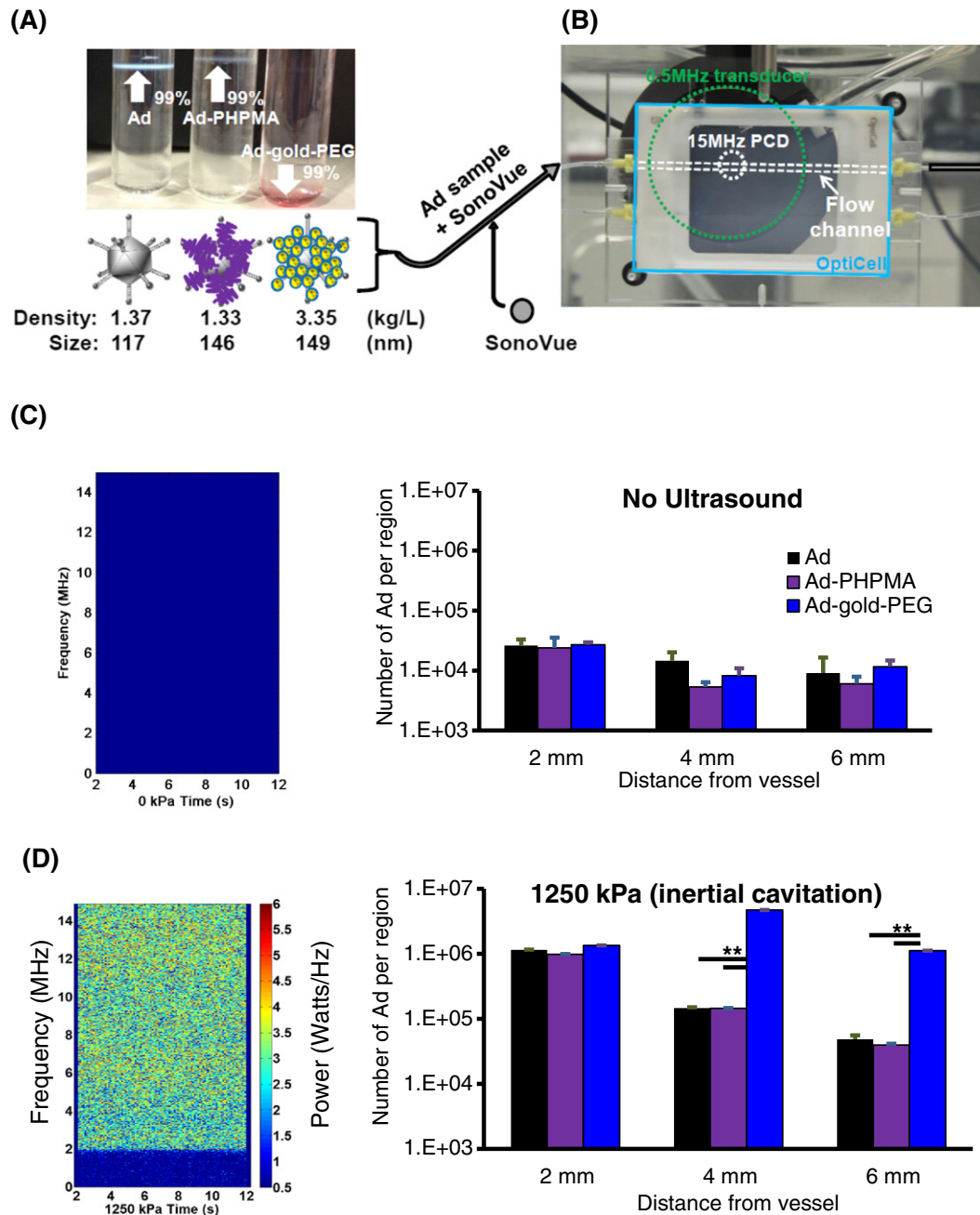
Fig. 4. Influence of increasing density on response to ultrasound. (A) Recovery of Ad, Ad–PHPMA and Ad–gold–PEG following ultracentrifugation through a caesium chloride density gradient. (B) In vitro ultrasound set-up, Ad sample and the ultrasound contrast agent SonoVue was applied via a flow channel through tissue mimicking material (TMM) containing cancer cells and exposed to ultrasound and the penetration of Ad into the TMM was measured. (C–D) Influence of ultrasound exposure on the penetration of Ad samples into TMM. The left panel shows a representative of the cavitation frequency spectra detected over the course of the 12 second ultrasound exposure as mapped using the passive cavitation detector. Broadband acoustic emissions in D are indicative of the occurrence of inertial cavitation. In the right panel the number of Ad recovered at different distances from the vessel was quantified using QPCR. N = 4, SD shown, ANOVA analysis performed.

ultrasound parameters provided no cavitation and no enhancement of virus transfer in the absence of SonoVue, and so this control was not included here.

In accordance with Fig. 3A, substantially reduced liver capture (29.3%, SD 2.14 vs 91.6% SD 8.36) was obtained with Ad–gold–PEG vs Ad, resulting in 35-fold increase in the circulating dose at 30 min (Fig. 5A). This provided a significant (p < 0.005) increase in tumour load of Ad–gold–PEG vs Ad, via passive accumulation (0.8% vs 0.1%). Notably, the level Ad–gold–PEG dose in the bloodstream following ultrasound exposure of the tumour was substantially lower compared to when ultrasound

was not applied (58% vs 69%), suggesting ultrasound-mediated mechanical transport of the Ad–gold–PEG out of the bloodstream. Indeed, the Ad–gold–PEG dose in ultrasound treated tumours proved to be significantly (p < 0.001) and substantially (14-fold) enhanced compared to non-ultrasound treated tumours (Fig. 5B). In total 12.2% (SD 0.97) of the dose of Ad–gold–PEG was recovered from ultrasound treated tumours. The previous highest level of ultrasound mediated enhanced uptake we have achieved was 3-fold using Ad–PHPMA [16], and never before has movement of dose into the tumour been so marked that it could be evidenced by loss of dose from the bloodstream. The combined benefit
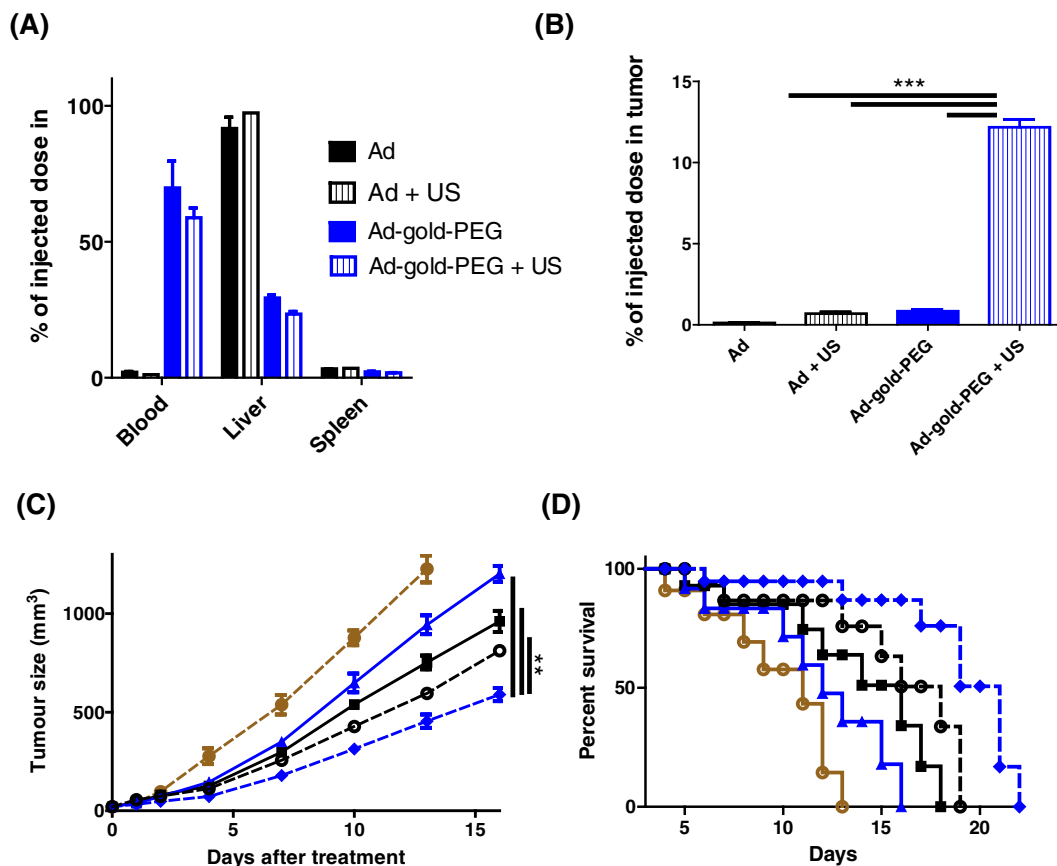
(A)

(B)

(C)

(D)

Fig. 5. Influence of ultrasound on mechanical transport to tumours. HepG2 tumour bearing CD-1 nude mice were injected with a single low dose (1×10^{10}) of oncolytic Ad or Ad–gold–PEG and tumours exposed to ultrasound or not and (A) bio-distribution and (B) tumour accumulation was measured at 30 min using QPCR, n = 4, SD shown, ANOVA analysis used. (C) In long term studies tumours were measured using callipers until a size of 1000 mm^3 was reached at which point mice were culled and (D) survival was plotted. Adenovirus genome content in tumours was measured at cull and related to day of cull. Brown circle = PBS, black square = Ad, black circle = Ad + ultrasound, blue triangle = Ad–gold–PEG, blue diamond = Ad–gold–PEG + ultrasound, N = 8, SD shown, ANOVA analysis or log rank test in (D).

of improved passive accumulation, (enhancing stealthing), and improved ultrasound induced cavitation-mediated mechanical transport, (enhancing particle density), provided more than 100-fold more Ad–gold–PEG within ultrasound treated tumours than Ad in non-ultrasound treated tumours. When the adenovirus luciferase reporter gene expression was measured at 24 h a 3-fold (p < 0.05) increase was observed in ultrasound treated tumours (Supplementary Fig. S7C), as in previous studies [16]. Notably luciferase expression was lower for Ad–gold–PEG without ultrasound than for Ad + ultrasound, despite equal levels of uptake. This may be the result of Ad–gold–PEG without ultrasound being deposited in well-perfused, non-reducing perivascular regions leading to inefficient uncoating and reactivation. Significant retardation of tumour growth was achieved in Ad–gold–PEG + ultrasound treated tumours (Fig. 5C) compared to all other groups. This lead to increased survival of Ad–gold–PEG + ultrasound treated mice compared to PBS, Ad, Ad + ultrasound or Ad–gold–PEG treated mice by log rank test (P = 0.0001, 0.0017, 0.0263, 0.0023 respectively) (Fig. 5D). Analysis of Ad genome copies present in tumours at cull (Supplementary Fig. S7D) revealed that Ad–gold–PEG + ultrasound treated tumours contained >50, 20 and 100-fold more Ad genomes than Ad, Ad + ultrasound or Ad–gold–PEG, which was the worst performing group perhaps indicating poor access to tumour regions in which effective un-coating of the gold–PEG and reactivation of infection could take place. This emphasises the importance of achieving improvements in mechanical transport into and throughout the tumour as well as EPR assisted passive increases in the total amount of tumour uptake, especially when 'phenotypic' low pH or reducing

conditions are relied upon for drug release or activation. Physical mechanisms such as ultrasound mediated cavitation are ideally suited to achieving improvements in delivery, as they are non-invasive, safe and can be monitored in real-time [40].

4. Discussion

Nanotechnologies are being developed to act as cancer drug delivery systems, including polymer, protein and lipid based nanomedicines [41, 42]. Direct administration into tumours is inefficient [43] and not always feasible, and so nanomedicines that are amenable to IV delivery are required. Regulation of size, shape, bloodstream stability and target site activation will be crucial to the success of these agents [13,44–46]. We report a "dandelion" structure of multi-PEGylated gold nanoparticles predominantly attached by a single reducible bond to the surface of the nanomedicine adenovirus. The chemistry underpinning this novel shielding methodology is in no way specific to adenovirus and so this is a widely applicable method of providing nanomaterials with improved protective steric shielding, without the requirement for activity compromising multivalent modification of their surface. This provides advantages over existing stealthing methodologies and allows improved protection against blood component binding. Furthermore, the inclusion of a disulphide bond in the linkage between Ad and the gold–PEG ensures that the activity of the nanomedicine can be recovered in a tumour-triggered manner. In pre-clinical models, Ad–gold–PEG had significantly longer circulation time, lower liver capture, and

increased tumour accumulation compared to Ad, Ad–PEG, and Ad–PHPMA. The ability of this design to substantially enhance passive tumour accumulation, makes it suitable for a future application in improving the efficiency and scope of a range of therapeutic and diagnostic nanotechnologies in the treatment of cancer including antibodies, peptides and nucleotides. In addition, as this stealthing method also allows the incorporation of nanoparticles, whether they are gold, carbon, iron oxide, or quantum dots, it may allow the power of nanomedicines to be combined with other new or clinically accepted nanoparticle based imaging modalities.

The second novel finding we describe relates to the increase in adenovirus particle density resulting from the linkage of gold–PEG and the impact increased density has upon response to focused ultrasound induced cavitation. We show that such inertial cavitation events can actively drive more Ad–gold–PEG to greater depths than similarly sized but less dense Ad or Ad–PHPMA. Furthermore, by controlling the ultrasound exposure parameters, the level of cavitation can be controlled and the degree and depth of Ad–gold–PEG penetration tuned, a process which is facilitated by the capacity to remotely map cavitation events as they occur using passive acoustic mapping [40]. This level of control and capacity for real-time feedback adds to the potential clinical utility of this approach. Indeed, tackling the physical barrier of high intratumoural pressure using a physical mechanism such as ultrasound has several distinct advantages over alternative chemical approaches such as vascular normalisation, which can even lead to the exclusion of nanoparticles from tumours [47]. The precise mechanism by which increasing the density of a nanotherapeutic enhances its cavitation-mediated delivery warrants further computational and experimental consideration. At the relatively low ultrasound frequency (0.5 MHz) and acoustic pressure (<1.5 MPa) used acoustic streaming is very weak and the nanotherapeutic is too small compared to the ultrasound wavelength to experience a substantial radiation force. The mechanism for delivery is therefore hypothesized to be microstreaming generated by sustained inertial cavitation, whereby the collapsing microbubble transfers momentum onto the surrounding liquid, which in turn entrains any nanoparticles suspended within it. The denser the nanoparticle, the more difficult it is for it to reach its terminal velocity, but the farther it will travel once that terminal velocity is reached due to having greater momentum than the surrounding liquid. We therefore hypothesize that a denser nanotherapeutic acquires momentum from the surrounding microstreaming fluid more effectively under conditions of sustained inertial cavitation.

5. Conclusions

We demonstrate that the passive accumulation and mechanical transport of a model nanomedicine adenovirus into tumours can be improved by the attachment of gold–PEG nanoparticles and the application of ultrasound to provide substantial enhancement to anti-tumour efficacy. This platform nanotechnology and these benefits could be applied to a wide range of nanomedicines.

Acknowledgements

Appendix A. Supplementary data

Supplementary data to this article can be found online at http://dx.doi.org/10.1016/j.jconrel.2015.05.265.

References

[1] J.W. Nichols, Y.H. Bae, Odyssey of a cancer nanoparticle: from injection site to site of action, Nano Today 7 (2012) 606–618.

[2] R. Laga, R. Carlisle, M. Tangney, K. Ulbrich, L.W. Seymour, Polymer coatings for delivery of nucleic acid therapeutics, J. Control. Release 161 (2012) 537–553.

[3] N. Bertrand, J.C. Leroux, The journey of a drug-carrier in the body: an anatomo-physiological perspective, J. Control. Release 161 (2012) 152–163.

[4] R.C. Carlisle, Y. Di, A.M. Cerny, A.F. Sonnen, R.B. Sim, N.K. Green, V. Subr, K. Ulbrich, R.J. Gilbert, K.D. Fisher, R.W. Finberg, L.W. Seymour, Human erythrocytes bind and inactivate type 5 adenovirus by presenting Coxsackie virus–adenovirus receptor and complement receptor 1, Blood 113 (2009) 1909–1918.

[5] A.L. Parker, S.N. Waddington, S.M. Buckley, J. Custers, M.J. Havenga, N. van Rooijen, J. Goudsmit, J.H. McVey, S.A. Nicklin, A.H. Baker, Effect of neutralizing sera on factor x-mediated adenovirus serotype 5 gene transfer, J. Virol. 83 (2009) 479–483.

[6] S.M. Moghimi, J. Szebeni, Stealth liposomes and long circulating nanoparticles: critical issues in pharmacokinetics, opsonization and protein-binding properties, Prog. Lipid Res. 42 (2003) 463–478.

[7] V. Subr, L. Kostka, T. Selby-Milic, K. Fisher, K. Ulbrich, L.W. Seymour, R.C. Carlisle, Coating of adenovirus type 5 with polymers containing quaternary amines prevents binding to blood components, J. Control. Release 135 (2009) 152–158.

[8] K. Doronin, E.V. Shashkova, S.M. May, S.E. Hofherr, M.A. Barry, Chemical modification with high molecular weight polyethylene glycol reduces transduction of hepatocytes and increases efficacy of intravenously delivered oncolytic adenovirus, Hum. Gene Ther. 20 (2009) 975–988.

[9] K. Ulbrich, R. Laga, V. Subr, Reactive polymers for modification of biologically active molecules and gene delivery vectors, J. Control. Release 116 (2006) e3–e5.

[10] Q. Yang, S.W. Jones, C.L. Parker, W.C. Zamboni, J.E. Bear, S.K. Lai, Evading immune cell uptake and clearance requires PEG grafting at densities substantially exceeding the minimum for brush conformation, Mol. Pharm. 11 (2014) 1250–1258.

[11] A. Danielsson, G. Elgue, B.M. Nilsson, B. Nilsson, J.D. Lambris, T.H. Totterman, S. Kochanek, F. Kreppel, M. Essand, An ex vivo loop system models the toxicity and efficacy of PEGylated and unmodified adenovirus serotype 5 in whole human blood, Gene Ther. 17 (2010) 752–762.

[12] K.M. Laginha, S. Verwoert, G.J. Charrois, T.M. Allen, Determination of doxorubicin levels in whole tumor and tumor nuclei in murine breast cancer tumors, Clin. Cancer Res. 11 (2005) 6944–6949.

[13] H. Cabral, Y. Matsumoto, K. Mizuno, Q. Chen, M. Murakami, M. Kimura, Y. Terada, M.R. Kano, K. Miyazono, M. Uesaka, N. Nishiyama, K. Kataoka, Accumulation of sub-100 nm polymeric micelles in poorly permeable tumours depends on size, Nat. Nanotechnol. 6 (2011) 815–823.

[14] H. Maeda, The enhanced permeability and retention (EPR) effect in tumor vasculature: the key role of tumor-selective macromolecular drug targeting, Adv. Enzym. Regul. 41 (2001) 189–207.

[15] S. Mo, C.C. Coussios, L. Seymour, R. Carlisle, Ultrasound-enhanced drug delivery for cancer, Expert Opin. Drug Deliv. 9 (2012) 1525–1538.

[16] R. Carlisle, J. Choi, M. Bazan-Peregrino, R. Laga, V. Subr, L. Kostka, K. Ulbrich, C.C. Coussios, L.W. Seymour, Enhanced tumor uptake and penetration of virotherapy using polymer stealthing and focused ultrasound, J. Natl. Cancer Inst. 105 (2013) 1701–1710.

[17] M. Bazan-Peregrino, B. Rifai, R.C. Carlisle, J. Choi, C.D. Arvanitis, L.W. Seymour, C.C. Coussios, Cavitation-enhanced delivery of a replicating oncolytic adenovirus to tumors using focused ultrasound, J. Control. Release 169 (2013) 40–47.

[18] G. Saito, J.A. Swanson, K.-D. Lee, Drug delivery strategy utilizing conjugation via reversible disulfide linkages: role and site of cellular reducing activities, Adv. Drug Deliv. Rev. 55 (2003) 199–215.

[19] W.G. Kirlin, J. Cai, S.A. Thompson, D. Diaz, T.J. Kavanagh, D.P. Jones, Glutathione redox potential in response to differentiation and enzyme inducers, Free Radic. Biol. Med. 27 (1999) 1208–1218.

[20] R.C. Carlisle, T. Bettinger, M. Ogris, S. Hale, V. Mautner, L.W. Seymour, Adenovirus hexon protein enhances nuclear delivery and increases transgene expression of polyethylenimine/plasmid DNA vectors, Mol. Ther. 4 (2001) 473–483.

[21] R. Cawood, S.L. Wong, Y. Di, D.F. Baban, L.W. Seymour, MicroRNA controlled adenovirus mediates anti-cancer efficacy without affecting endogenous microRNA activity, PLoS One 6 (2011) e16152.

[22] R.A. Willemsen, M. Pechar, R.C. Carlisle, E. Schooten, R. Pola, A.J. Thompson, L.W. Seymour, K. Ulbrich, Multi-component polymeric system for tumour cell-specific gene delivery using a universal bungarotoxin linker, Pharm. Res. 27 (2010) 2274–2282.

[23] C.E. Aitken, R.A. Marshall, J.D. Puglisi, An oxygen scavenging system for improvement of dye stability in single-molecule fluorescence experiments, Biophys. J. 94 (2008) 1826–1835.

[24] T.Y. Aw, Cellular redox: a modulator of intestinal epithelial cell proliferation, Physiology 18 (2003) 201–204.

[25] F. Kreppel, S. Kochanek, Modification of adenovirus gene transfer vectors with synthetic polymers: a scientific review and technical guide, Mol Ther 16 (2008) 16–29.

[26] N.K. Green, C.W. Herbert, S.J. Hale, A.B. Hale, V. Mautner, R. Harkins, T. Hermiston, K. Ulbrich, K.D. Fisher, L.W. Seymour, Extended plasma circulation time and decreased toxicity of polymer-coated adenovirus, Gene Ther. 11 (2004) 1256–1263.

[27] H. Chen, J.H. Hwang, Ultrasound-targeted microbubble destruction for chemotherapeutic drug delivery to solid tumors, J. Ther. Ultrasound 1 (2013) 10.

[28] O.M. Pearce, K.D. Fisher, J. Humphries, L.W. Seymour, A. Smith, B.G. Davis, Glycoviruses: chemical glycosylation retargets adenoviral gene transfer, Angew. Chem. 44 (2005) 1057–1061.

[29] M.J. Cotter, A.K. Zaiss, D.A. Muruve, Neutrophils interact with adenovirus vectors via Fc receptors and complement receptor 1, J. Virol. 79 (2005) 14622–14631.

[30] M.A. Croyle, N. Chirmule, Y. Zhang, J.M. Wilson, PEGylation of E1-deleted adenovirus vectors allows significant gene expression on readministration to liver, Hum. Gene Ther. 13 (2002) 1887–1900.

[31] N.K. Green, A. Hale, R. Cawood, S. Illingworth, C. Herbert, T. Hermiston, V. Subr, K. Ulbrich, N. van Rooijen, L.W. Seymour, Tropism ablation and stealthing of oncolytic adenovirus enhances systemic delivery to tumors and improves virotherapy of cancer, Nanomedicine (2012) 1–13.

[32] E. Wisse, F. Jacobs, B. Topal, P. Frederik, B. De Geest, The size of endothelial fenestrae in human liver sinusoids: implications for hepatocyte-directed gene transfer, Gene Ther. 15 (2008) 1193–1199.

[33] R. Alemany, K. Suzuki, D.T. Curiel, Blood clearance rates of adenovirus type 5 in mice, J. Gen. Virol. 81 (2000) 2605–2609.

[34] N.K. Green, A. Hale, R. Cawood, S. Illingworth, C. Herbert, T. Hermiston, V. Subr, K. Ulbrich, N. van Rooijen, L.W. Seymour, K.D. Fisher, Tropism ablation and stealthing of oncolytic adenovirus enhances systemic delivery to tumors and improves virotherapy of cancer, Nanomedicine (London) 7 (2012) 1683–1695.

[35] M.G.-M. Emiliano Calvo, Jean-Pascal H. Machiels, Sylvie Rottey, Antonio Cubillo, Ramon Salazar, Feby Ingriani Mardjuadi, Karen Paula Geboes, Christopher Ellis, John William Beadle, Christine Blanc, A first-in-class, first-in-human phase I study of enadenotucirev, an oncolytic Ad11/Ad3 chimeric group B adenovirus, administered intravenously in patients with metastatic epithelial tumors, J. Clin. Oncol. 32 (2014) (abstr TPS3112).

[36] S. Wang, I.S. Shin, H. Hancock, B.S. Jang, H.S. Kim, S.M. Lee, V. Zderic, V. Frenkel, I. Pastan, C.H. Paik, M.R. Dreher, Pulsed high intensity focused ultrasound increases penetration and therapeutic efficacy of monoclonal antibodies in murine xenograft tumors, J. Control. Release 162 (2012) 218–224.

[37] S.M. Graham, R. Carlisle, J.J. Choi, M. Stevenson, A.R. Shah, R.S. Myers, K. Fisher, M.B. Peregrino, L. Seymour, C.C. Coussios, Inertial cavitation to non-invasively trigger and monitor intratumoral release of drug from intravenously delivered liposomes, J. Control. Release 178 (2014) 101–107.

[38] M. Kendall, T. Mitchell, P. Wrighton-Smith, Intradermal ballistic delivery of micro-particles into excised human skin for pharmaceutical applications, J. Biomech. 37 (2004) 1733–1741.

[39] C.D. Arvanitis, M. Bazan-Peregrino, B. Rifai, L.W. Seymour, C.C. Coussios, Cavitation-enhanced extravasation for drug delivery, Ultrasound Med. Biol. 37 (2011) 1838–1852.

[40] J.J. Choi, R.C. Carlisle, C. Coviello, L. Seymour, C.C. Coussios, Non-invasive and real-time passive acoustic mapping of ultrasound-mediated drug delivery, Phys. Med. Biol. 59 (2014) 4861–4877.

[41] D. Peer, J.M. Karp, S. Hong, O.C. Farokhzad, R. Margalit, R. Langer, Nanocarriers as an emerging platform for cancer therapy, Nat. Nanotechnol. 2 (2007) 751–760.

[42] Y. Barenholz, Doxil(R) — the first FDA-approved nano-drug: lessons learned, J. Control. Release 160 (2012) 117–134.

[43] M. Bazan-Peregrino, R.C. Carlisle, L. Purdie, L.W. Seymour, Factors influencing retention of adenovirus within tumours following direct intratumoural injection, Gene Ther. 15 (2008) 688–694.

[44] Y. Geng, P. Dalhaimer, S. Cai, R. Tsai, M. Tewari, T. Minko, D.E. Discher, Shape effects of filaments versus spherical particles in flow and drug delivery, Nat. Nanotechnol. 2 (2007) 249–255.

[45] Y. Barenholz, Nanomedicine: shake up the drug containers, Nat. Nanotechnol. 7 (2012) 483–484.

[46] T. Lammers, F. Kiessling, W.E. Hennink, G. Storm, Drug targeting to tumors: principles, pitfalls and (pre-) clinical progress, J. Control. Release 161 (2012) 175–187.

[47] V.P. Chauhan, T. Stylianopoulos, J.D. Martin, Z. Popovic, O. Chen, W.S. Kamoun, M.G. Bawendi, D. Fukumura, R.K. Jain, Normalization of tumour blood vessels improves the delivery of nanomedicines in a size-dependent manner, Nat. Nanotechnol. 7 (2012) 383–388.